Latex Particle Heterogeneity and Clustering in Films

Érico Teixeira-Neto,[†] Gerd Kaupp,[‡] and Fernando Galembeck*,[†]

Instituto de Química, Universidade Estadual de Campinas, UNICAMP, PO Box 6154, CEP 13084-971, Campinas, SP, Brazil, and Universität Oldenburg, Organische Chemie I, Postfach 2503, D-26111 Oldenburg, Germany

Received: June 17, 2003; In Final Form: October 16, 2003

A poly(styrene-*co*-acrylamide) (PS-AAM) latex was prepared by emulsion polymerization and purified by sedimentation of colloidal crystals. These were diluted and dried on a mica substrate forming submonolayers that were examined by atomic force microscopy (AFM), scanning electron microscopy (SEM), and near-field optical microscopy (SNOM). The images show domains of at least two particle types clustered within the films, in every field examined. Zonal centrifugation of the colloidal-crystal forming particles still produced three separated fractions, two of which were further cast into uniform submonolayers. These results show that latex particles have a strong tendency to cluster with identical particles even in the presence of other, similar particles. However, colloidal crystal formation has a limited tolerance to particle heterogeneity but the quality of the dry macrocrystals is strongly dependent on particle uniformity.

1. Introduction

Copolymer latexes[1] produced by emulsion polymerization[2] have a large and still growing importance as model colloids and industrial products and intermediates. The emulsion polymerization process is affected by many factors that affect chain polymerization, creating a great diversity within copolymer chains.[3] The different chain types thus generated would then tend to cluster, forming different particle sub-populations. The particle nucleation is not always fully reproducible, and successive polymerizations using the same recipe may give particles with different characteristics.[4] It depends on many factors such as polarity and reactivity[5] of the monomers, type of initiator,[6] and the rate of radical generation. For this reason, latex particles should display some degree of heterogeneity concerning their detailed chemical composition, size and properties.[7,8] Changing polymerization regimes have been demonstrated, and they can lead to differentiated particles.[9] MW and chain composition modeling[10−14] have been done extensively. Modeling of particle growth and morphology[15] has also been done with a good agreement with experimental results.[16−19] This often requires significant computation effort, because there is a large number of kinetic and partitioning parameters involved. On the other hand, particle composition modeling does not seem to have been attempted, to the best of our knowledge.

The physical and chemical properties of the particle films may be affected by the nonuniform distribution of particle sub-populations within the films, if these will form distinct domains with different properties (e.g., adhesion, permeation, sweling). Previous work from this laboratory showed that the quality of self-assembled particle arrays is dependent on the uniformity of the latex particles and the quality of macrocrystals was much improved by latex fractionation, in the cases of poly(styrene-*co*-hydroxyethylmetacrylate)[20] and poly(styrene-*co*-acrylamide)[21] (PS-AAM). This means that increasing particle homogeneity with the exclusion of "impurity" particles of different size or chemical composition[22] is a feasible and convenient approach for the fabrication of highly ordered macrocrystals. Unexpected coagulation behavior has been assigned to the existence of minor sub-populations within a latex, because of the reaction occurring in different reactor compartments.[3]

There are now many accurate and fast techniques for particle and macromolecular chain size determinations.[23] Centrifugation in density gradients has been particularly helpful not only in demonstrating the existence of different fractions within many types of latexes but also as a preparative technique, to produce highly homogeneous latex fractions.[24] On the other hand, particle chemical heterogeneity within films is not normally assessed, except in a few cases in which transmission electron microscopy can be used to yield information about the distribution of constituents within the particles.[22]

Given the existence of chemically different particle sub-populations within a latex, a new question may be raised: do similar particles cluster, forming separate domains within a latex coagulum or film? Clustering of particle sub-populations during film drying is to be expected, considering that the van der Waals particle−particle attraction is expected to be highest for particles of identical composition rather than for particles with greater chemical differences, because the Hamaker constants of the former will also be more similar than for the latter.[25]

The observation of particle clustering according to their chemical similarities within the latex dispersion is experimentally more difficult than in coaguli or dry films, because of particle mobility within the dispersion and also because there are more spatially resolved analytical techniques suitable for solids than for liquids. However, even within liquids there is the possibility for colloidal phase separation[26−29] within a dispersion, which creates large local changes in particle concentration, independent of any particle chemical heterogeneity. Colloidal phase separation is dependent on interparticle potentials, consequently different particle sub-populations are expected to phase-separate under different conditions. Together, all of these factors should create film heterogeneities, but these have not been shown explicitly, in the literature.

* To whom correspondence should be addressed. E-mail: fernagal@iqm.unicamp.br.
[†] Universidade Estadual de Campinas.
[‡] Universität Oldenburg.

10.1021/jp035718q CCC: $25.00
Published on Web 11/26/2003

This work presents microscopy evidence on particle clustering within self-arrayed PS-AAM films, showing that particles with very similar diameter and chemical composition are indeed separated and clustered into differentiated domains.

2. Experimental Section

2.1. Latex Preparation. The latex was synthesized by batch surfactant-free emulsion copolymerization of styrene (S) and acrylamide (AAM) following a procedure similar to that used by Tamai et al.[30] Following the synthesis, the latex was purified by filtration, to remove coagulated latex, and then by dialysis with water with two daily changes over a 35-day period, to remove unreacted monomer, oxidation products and unwanted electrolyte.

2.2. Latex Fractionation. *2.2.1. Latex Fractionation under Gravity.* After the purification, 200 mL of the latex were stored in a 250 mL closed glass container and fractionated under gravity. Within few months, a thick opalescent layer was easily observed in the bottom of the container. The color of reflected light changed markedly with the observation angle and the domains showing a uniform color extended for many millimeters, evidencing the formation of macroscopic colloidal crystals. The opalescent layer was separated by a definite interface from an opaque, milky layer just above it. A second interface was observed between the milky layer and a translucent dispersion at the top of the liquid. The experiments performed in this work were done on samples collected from the opalescent bottom fraction (Bt), 45 months after this latex was prepared and stored. A detailed characterization of this latex was published elsewhere.[21]

2.2.2. Zonal Centrifugation in Density Gradients. The Bt fraction was further fractionated by zonal centrifugation in a density gradient. The experiments were done by layering 100 μL latex zones (1% w/w) on top of preformed linear sucrose density gradients, prepared mixing water and 20% aqueous sucrose,[31] followed by centrifugation at 5 krpm for 4 h in a Sorvall RC3B centrifuge. The densities of the bands obtained were determined by imaging the centrifuge tubes with a digital camera and line-scanning the tube pictures, along the tube axis, for the acquisition of scattered light profiles with the Image-Pro Plus 4.0 (Media Cybernetics) software. After centrifugation, the bands were carefully collected with syringes fitted with long glass tips, to avoid cross-contamination. Bands containing the latex sub-fractions were then dialyzed to remove sucrose by centrifugal ultrafiltration[32] at 3 krpm using acrylic cells with cellulose acetate membranes.

2.3. Particle Effective Diameter and Zeta-Potential Determinations. Particle effective diameter and zeta potential determinations were made by photocorrelation spectroscopy (PCS) using a ZetaPlus Brookhaven Instrument fitted with BI-MAS software. Zeta potential determinations were performed using platinum electrodes within square cells made of acrylic polymer, using latex samples diluted with 10^{-3} mol L^{-1} aqueous KCl.

2.4. Infrared Spectroscopy. Infrared spectra were obtained with a Bomem MB Series 102 spectrophotometer. The samples were analyzed in the form of tablets, with KBr as dispersing solid.

2.5. Sample Preparation for Microscopy. Particle films were prepared from the PS-AAM Bt fraction and from its sub-fractions by depositing 100 μL of the dispersions on freshly cleaved mica sheets and allowing the dispersions to dry under 60−70% relative humidity at 25 ± 2 °C. Solid contents of the PS-AAM dispersions used to prepare the samples were 10% w/w for macrocrystals and 0.1% w/w for submonolayers.

2.6. Microscopy Techniques. *2.6.1. High-Resolution Scanning Electron Microscopy (FESEM).* Secondary electron images (SEI) were acquired in a JEOL JSM 6340F field-emission scanning electron microscope, operating at 5 kV. The samples were placed on brass stubs and carbon-coated in a Bal-Tec MD 020 instrument, for FESEM imaging. The microscope was calibrated with a 25 μm Ni square grid standard. Image processing was performed using the Image-Pro Plus 4.0 (Media Cybernetics) software.

2.6.2. Atomic Force Microscopy (AFM). AFM images were acquired in a Topometrix Discoverer scanning probe microscope. A noncontact AFM mode was used to obtain topographic information on the particle films. Samples on mica were glued to specific instrument sample holders for examination under air. Topographic changes were sensed by monitoring the detector signal amplitude at 300 × 300 pixel resolution and 10 μm/s scan rate. The instrument was calibrated with a standard grid formed by a regular array of 0.9 μm spaced SiO_2 cylinders with diameter of 1.1 μm and height of 240 nm, on the Si surface. The probes used were made of silicon coated with platinum and had a pyramidal shape with a spherical 20 nm nominal radius tip, which was verified by imaging the tip in the field-emission scanning electron microscope. Image processing was performed in a PC microcomputer using the Topometrix analysis program. A first order plane-fit leveling was applied along the plane of the mica substrate in the images. Height distribution histograms of selected low-pass filtered areas were acquired using the Image-Pro Plus 4.0 (Media Cybernetics) software.

2.6.3. Scanning Near Field Optical Microscopy (SNOM). A SNOM DME Rasterscope 4000 in a reflection-back-to-fiber configuration was used to acquire topographical and optical information on the particle films surface. In this configuration, an uncoated optical fiber tip is used to simultaneously illuminate and detect the evanescent field generated at the sample surface.[33−35] Tapered optical fiber probes suitable for SNOM imaging[36] were produced through a multistage heating-pulling process using a programmable micropipet puller P-2000 (Sutter Instruments). Examination of the obtained tips in a field-emission gun scanning electron microscope indicates tip curvature radii of 13.3 nm and cone angle of 5.8°. An argon-ion laser (488 nm) coupled into the fiber was used to illuminate the sample. The near-field enhanced[33−35] reflected light was detected through a cross-polarized detection setup in order to remove stray light and to record the chemical contrast of the sample surface. The tip-to-sample shear-force gap was kept constant while scanning. In the shear-force microscopy (ShFM) technique[37] used, the fiber probe was oscillated at its mechanical resonance frequency (10−200 kHz), and upon approaching the sample surface, attractive van der Waals forces or water layers acting on the tip caused a reduction of its vibration amplitude. A laser beam was focused on the vibrating fiber tip and the modulation of its shadow was detected on a photodiode, thus monitoring the vibration amplitude. The amplitude reduction was compared with some preset value, and the resulting difference was fed back to the *z* piezo so as to adjust the probe tip-to-sample shear-force separation. The signal variation of the *z* piezo while scanning was used to build a topographic image (ShFM) simultaneously to the optical image (SNOM), with 512 × 512 pixels resolution and at 10 μm/s scan rate. A first order plane-fit leveling was applied along of the plane of the mica substrate in the images. Image processing was performed using the Image-Pro Plus 4.0 (Media Cybernetics) software.

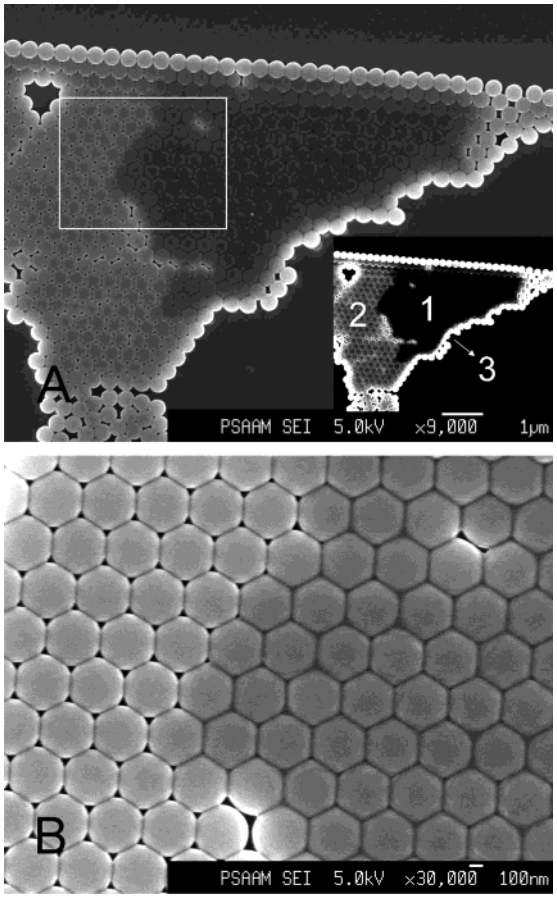

Figure 1. (A) SEI micrograph of a PS-AAM bottom fraction particle submonolayer. (B) Enlarged view of the area delimited by the white rectangle in image A. The inset in image A is a high-contrast copy of the micrograph A, showing the position of the domains described in the text.

3. Results

The PS-AAM latex shows significant particle chemical heterogeneity, which was described in detail in a previous work.[21] The following results were obtained using the fraction separated by colloidal crystallization, which is expected to be highly homogeneous.

Figure 1 shows SEM images of a particle submonolayer of the PS-AAM Bt fraction.

In Figure 1A, it is possible to identify at least three domains made out of different particle types: (1) densely packed hexagonal particles darker than their neighbors, which occupy a mean area per particle of 0.142 μm^2 in the image plane; (2) densely packed particles with a distorted circular projection in the image plane and a mean area per particle of 0.145 μm^2, uniformly brighter than the former; (3) particles at the array border and around its defects, with larger mean area per particle in the image plane (0.150 μm^2) than the others. The last group makes a smaller population, since it is found only at the aggregate borders.

All particles are within the image area (ca. 142 μm^2), and consequently, they acquired their different aspects within very uniform drying and imaging conditions and their appearance can be used to compare their morphogenetic properties. Figure 1B shows the area delimited by a rectangle in Figure 1A, but with a higher resolution. The particles of the dark domain are very plastic, and their hexagonal shape shows that they were highly compliant to the efforts made by capillary adhesion, during film drying. A few particles are observed in defects

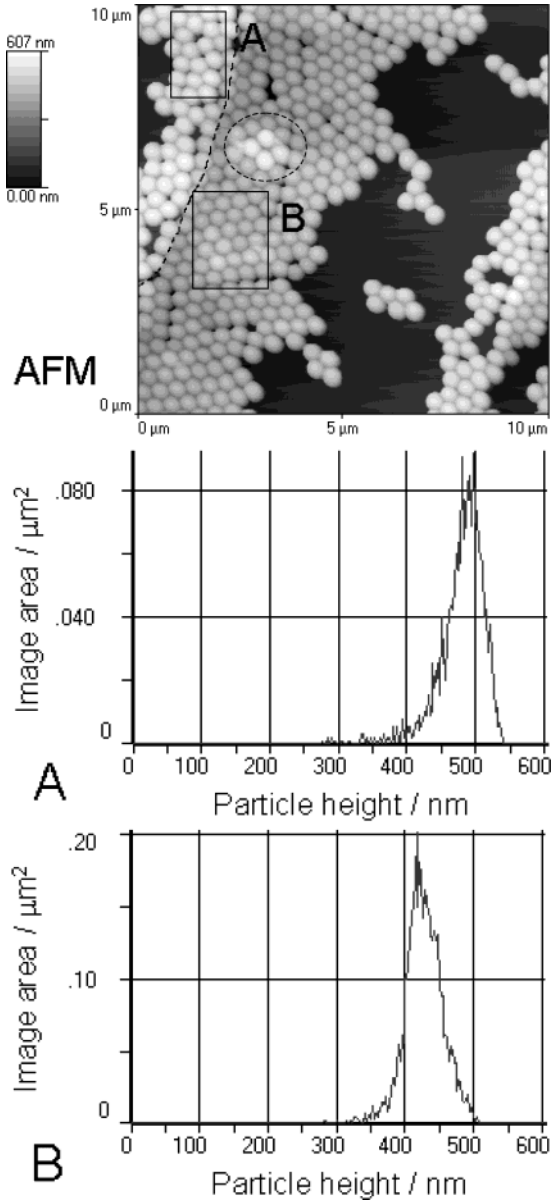

Figure 2. Noncontact AFM image of a PS-AAM bottom fraction particle submonolayer and histograms of particle height distribution within the areas delimited by the black rectangles drawn in the image.

within this domain: they have bright border spots that are undeformed. The particles of the brighter domain are only partially deformed into hexagons, and consequently, either they are less plastic than the former or they are less wetted by the residual drying serum, so that the capillary adhesion forces are weaker and thus unable to completely pull them into hexagonal shapes.

The submonolayer of PS-AAM Bt fraction particles in the AFM image of Figure 2 shows three different types of particle domains. The first is formed by bright (and thus taller) particles with a low degree of ordering, to the left of the dashed line, while the second contains darker particles hexagonally ordered to the right of the dashed line. Finally, there is a group of four very bright particles, in the area delimited by the dashed ellipse drawn in the image, arranged in a segregated domain of particles within another domain. Height measurements show that this small cluster is *not* on top of the particle monolayer.

The histograms in Figure 2 show the distribution of height from the particles within the image areas delimited by the

TABLE 1: Particle Effective Diameter, Zeta Potential, and Isopycnic Densities for the Latex Fractions Studied

latex fraction	bottom fraction[a]	fraction A[b]	fraction B[b,c]	fraction C[b]
effective diameter (nm)	457 ± 8	467 ± 1		450 ± 5
zeta potential (mV)	-35.8 ± 0.4	-34.3 ± 0.8		-33.6 ± 0.9
isopycnic density (g cm^{-3})		1.046−1.047	1.050	1.056−1.058

[a] Collected from the bottom of the container in which the latex was stored, following its preparation. [b] The bottom fraction was further fractionated by zonal centrifugation, yielding the sub-fractions A−C. [c] Fraction B was not recovered owing to its low amount.

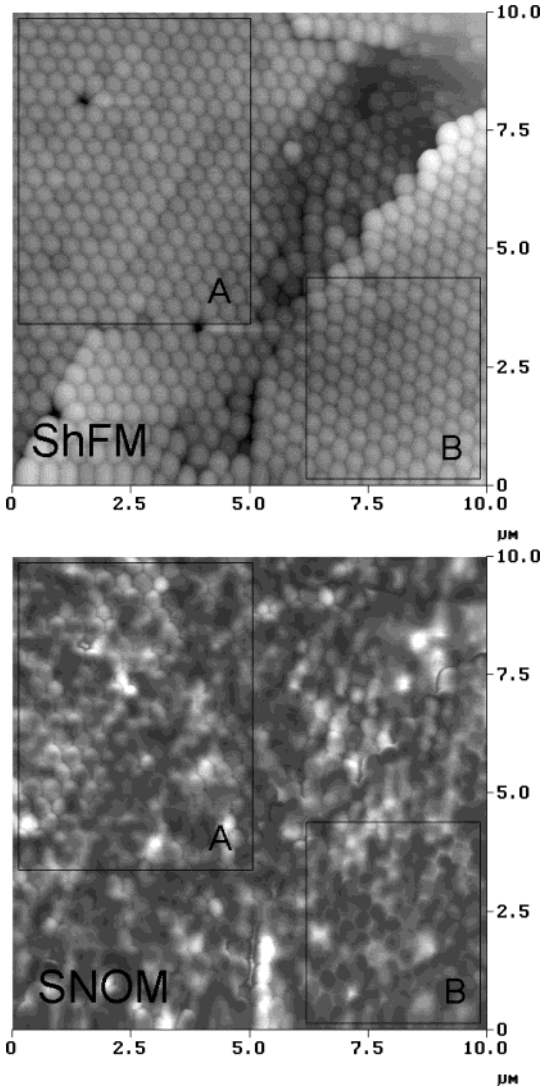

Figure 3. ShFM and SNOM images of the surface of a thick PS-AAM bottom fraction macrocrystal.

rectangles A and B, from the bright and darker domains, respectively. The particles within the rectangle A have an average height of 479 nm, higher than the hexagonally ordered particles within the rectangle B, which have an average height of 418 nm. Thus, the higher particles within the bright domain have different packing behavior than the darker particles from the darker domain, pointing to the differences in their physicochemical properties and, consequently, to their different chemical compositions.

The ShFM-SNOM images in Figure 3 are from the surface of a PS-AAM thick macrocrystal, prepared with the latex Bt fraction.

The particles within the A and B rectangles are hexagonally packed in the ShFM image of Figure 3. In the rectangle A of the SNOM image, the particle outer areas are darker than the particle central areas, but within rectangle B, the particles are darker than the interparticle domains. The brightness difference observed between the particles within the rectangles A and B is a result of the difference in the evanescent wave intensity generated at the surface of both particle domains, which is assigned to the chemical and morphological differences between these particles.

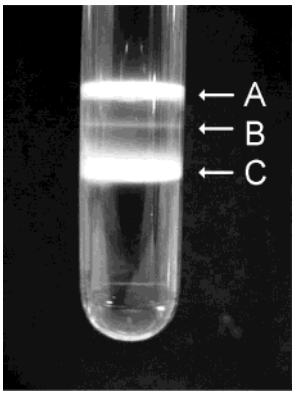

Figure 4. Picture of a density gradient tube after a PS-AAM fractionation experiment.

The previous results show that the bottom fraction of the PS-AAM latex still contains sub-populations with highly different packing abilities, even though the bottom fraction is sufficiently uniform to easily undergo latex crystallization. To achieve more uniform latex fractions, the Bt fraction was subjected to zonal centrifugation in a sucrose density gradient.

Figure 4 shows a picture of a density gradient tube after a PS-AAM fractionation experiment.

Three sub-fractions named A, B, and C were obtained under isopycnic conditions; particle effective diameters, zeta potentials, and isopycnic densities are in Table 1.

The particles from sub-fraction A have a bigger effective diameter and a lower isopycnic density than the particles from sub-fraction C, evidencing that the PS-AAM Bt fraction is indeed composed by well-defined particle sub-populations, with definite physical and chemical differences between them. However, the C band in Figure 4 is broader than the A band, showing that C is still more heterogeneous than A.

Infrared spectra of the bottom fraction (Bt) and of the sub-fractions A and C are presented in Figure 5.

The spectra of the Bt fraction and from its two sub-fractions (A and C) are very similar. The absorbances at 1654 (C═O stretching) and 1420 and 1105 cm^{-1} (C−N stretching) are all due to acrylamide. The ratios of the absorbances at 1654 and 1493 cm^{-1} (ϕ−R deformation, from the aromatic ring in styrene) in the sub-fractions A and C are respectively 0.51 and 0.42. The sub-fraction A particles are thus richer in acrylamide and consequently more hydrophilic than the sub-fraction C particles; this causes the A particles to be swollen by water, increasing their diameter and thus decreasing their density, as observed in Table 1.

Figure 6 shows a submonolayer of hexagonally ordered particles from the sub-fraction A.

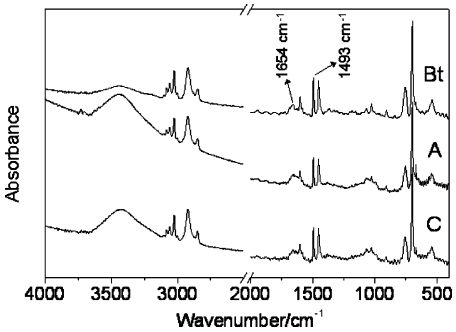

Figure 5. Infrared spectra from the PS-AAM bottom fraction and from its sub-fractions A and C.

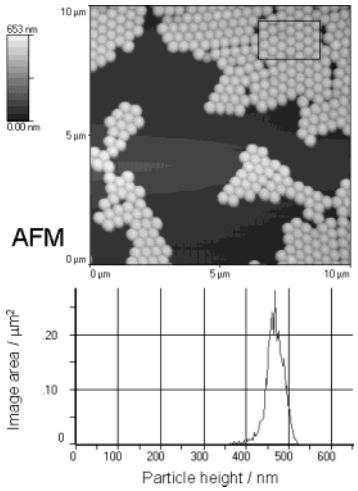

Figure 6. Noncontact AFM image of a PS-AAM sub-fraction A particle submonolayer on mica and histogram of particle height distribution within the area delimited by the black rectangle drawn in the image.

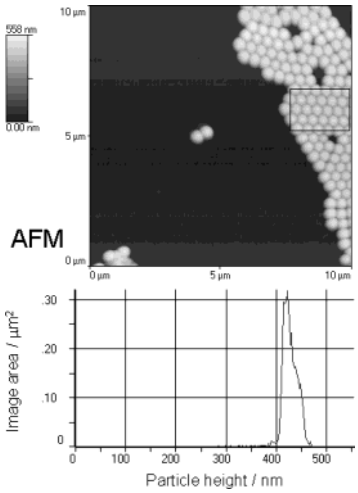

Figure 7. Noncontact AFM image of a PS-AAM sub-fraction C particle submonolayer on mica and histogram of particle height distribution within the area delimited by the black rectangle drawn in the image.

The brightness of the particles is evenly distributed, as opposed to Figure 1, thus evidencing the existence of a fairly uniform particle sub-population. The height distribution histogram of the area delimited by the rectangle drawn in the image shows a 467 nm mean particle height.

In Figure 7, the AFM image from C sub-fraction particles also shows a regular distribution of brightness. The histogram from the area delimited by the rectangle drawn in the image shows a mean height equal to 422 nm.

4. Discussion

The sample used in this work produces strongly opalescent latex crystals, which is often associated with particle homogeneity, but the images show that within this seemingly homogeneous latex there are still sub-fractions detected by microscopy. Particle separation and clustering are expected within a latex containing different sub-populations of particles differentiated by their chemical compositions, because the interparticle interactions are different for two reasons: first, the attractive contribution to particle interactions are dependent on chemical composition, so that they should be stronger for particles within a given sub-population than for particles from different sub-populations; second, the repulsive (electrostatic, steric, and hydration) contributions are also dependent on particle composition and the outcome is that "like attracts like", as in many other chemical systems. Following theoretical models such as that recently presented by Lai and Wu,[25] the particles are clustered within the dispersion due, e.g., to the onset of liquid−liquid and liquid−solid phase separations and they remain in separated domains in the drying process, so that the particle clusters are indeed experimentally detected side by side or interspersed, as shown in the micrographs presented in this work. It is remarkable that even very similar particles can still be distinguished within a dispersion fraction for their ability to cluster with their kin, reducing contact with particles of different compositions.

The three different techniques used (AFM, SEM, and SNOM) equally detected the coexistence of particle clusters though by using different properties: topography (AFM), ability for secondary electron emission (SEM), particle packing geometry (AFM and SEM), and evanescent wave intensity (SNOM).

Among these techniques, SNOM has the greatest sensitivity to minute differences in particle chemical composition within a particle cluster, as evidenced by the contrast pattern in Figure 3. This is comparable to the complexity revealed by backscattered detection in the scanning electron microscope (SEM-BEI)[38] and scanning electric potential microscopy (SEPM).[39]

The clustering patterns presented in this work show that great caution should be exerted whenever latexes are used as model colloids or even as models for phase separation, glass transition, and other basic physicochemical phenomena. To avoid misinterpretations of the phenomena observed, an experimental demonstration of particle uniformity is needed, and this cannot be achieved without previous latex fractionation followed by a careful characterization of the fractions prior to their use in further experimentation, as shown in the centrifugation experiment described in this work and in the subsequent particle characterization. The data for the sub-populations are all consistent, especially the average particle heights: 479 and 418 nm in the unfractionated sample in Figure 2, as compared to 467 (sub-fraction A) and 422 nm (sub-fraction C) in Figures 6 and 7.

Comparing the AFM data with the particle diameters in Table 1, there is a better agreement for A than for C. This is the opposite of the expected result, considering that A is richer in acrylamide than C. Consequently, A swelled to a higher extent so that its PCS diameter (measured within water) was found to be significantly higher than in AFM measurements, scanned on dry particles. However, this comparison must not be overstressed, because the present AFM results refer to a small number of particles only, and they do not have the same statistical significance as the PCS data.

Particle clustering should affect the mechanical, swelling and optical latex film properties and the properties determined by

macroscopic techniques are thus to be seen only as weighted averages of cluster properties.

Finally, this shows that the use of microscopy techniques may be misleading, if the experimenter does not examine many different fields of any sample of interest. This is especially important wherever longer image acquisition times make multiple image acquisition more difficult and time-consuming.

5. Conclusions

The PS-AAM latex sample investigated in this work consists of different sub-populations of particles with different physicochemical properties. These particle sub-populations autosegregate themselves during film formation, yielding separated domains of particles with similar characteristics, as determined using the SEI, AFM, and SNOM microscopy techniques. Further fractionation of this PS-AAM sample yielded more homogeneous particle sub-populations, pointing to the requirement of a detailed characterization of any latex preparation before using it as a model colloid.

Acknowledgment. F.G. acknowledges the support of FAPESP, CNPq/PADCT (Millenium Institute of Complex Materials) and Pronex/Finep/MCT. E.T.-N. is supported by a Fapesp pre-doctoral fellowship.

References and Notes

(1) Buscall, R.; Ottewill, R. H. *Polymer Colloids*; Elsevier: London, 1985; Chapter 5.
(2) Napper, D. H.; Gilbert, R. G. In *Comprehensive Polymer Science*; Ledwith, A., Russo, S., Sigwalt, P., Eds.; Pergamon: London, 1989; Vol. 4, pp 171−218.
(3) Vanderhoff, J. W. *Chem. Eng. Sci.* **1993**, *48*, 203.
(4) Snupárek, J.; Bradna, P.; Mrkvicková, L.; Lednick×c6, F.; Quadrat, O. *Collect. Czech. Chem. Commun.* **1993**, *58*, 2451.
(5) Fitch, R. M. *Polymer Colloids: A Comprehensive Introduction*; Academic Press: London, 1997.
(6) Van Hamersveld, E. M. S.; Van Es, J. J. G. S.; German, A. L.; Cuperus, F. P.; Weissenborn, P.; Hellgren, A.-C. *Prog. Org. Coat.* **1999**, *35*, 235.
(7) Galembeck, F.; Souza, E. F. In *Polymer Interfaces and Emulsions*; Esumi, K., Ed.; Marcel Dekker: New York, 1999; p 119.
(8) Neto, J. M. M.; Cardoso, A. L. H.; Testa A. P.; Galembeck, F. *Langmuir* **1994**, *10*, 2095.
(9) Lin, S. Y.; Capek, I.; Hsu, T. J.; Chern, C. S. *J. Polym. Sci. A* **1999**, *37*, 4422.
(10) Ma, J. W.; Cunningham, M. F.; McAuley, K. B.; Keoshkerian, B.; Georges, M. *Chem. Eng. Sci.* **2003**, *58*, 1177.
(11) Othman, S.; Barudio, I.; Fevotte, G.; McKenna, T. F. *Polym. React. Eng.* **1999**, *7*, 1.
(12) Platkowski, K.; Reichert, K. H. *Polymer* **1999**, *40*, 1057.
(13) Platkowski, K.; Pross, A.; Reichert, K. H. *Polym. Intern.* **1998**, *45*, 229.
(14) Hernandez-Barajas, J.; Hunkeler, D. J. *Polymer* **1997**, *38*, 437.
(15) Ferguson, C. J.; Russel, G. T.; Gilbert, R. G. *Polymer* **2002**, *43*, 4557.
(16) De la Cal, J. C.; Asua, J. M. *J. Polym. Sci. A* **2001**, *39*, 585.
(17) Dougherty, E. P. *J. Appl. Polym. Sci.* **1986**, *32*, 3051.
(18) Dougherty, E. P. *J. Appl. Polym. Sci.* **1986**, *32*, 3079.
(19) Saldivar, E.; Dafniotis, P.; Ray, W. H. *J. Macromol. Sci.* **1998**, *C38*, 207.
(20) Cardoso, A. H.; Leite, C. A. P.; Galembeck, F. *J. Braz. Chem. Soc.* **1999**, *10*, 497.
(21) Teixeira-Neto, E.; Leite, C. A. P.; Cardoso, A. H.; Silva, M. C. V. M.; Braga, M.; Galembeck, F. *J. Colloid Interface Sci.* **2000**, *231*, 182.
(22) Cardoso, A. H.; Leite, C. A. P.; Galembeck, F. *Langmuir* **1998**, *14*, 3187.
(23) Hunter, R. J. *Foundations of Colloids Science*; Oxford: Belfast, 1991; Vol. 1.
(24) Winkler-Hechenleitner, A. A.; Galembeck, F. *Sep. Sci. Technol.* **1990**, *25*, 293.
(25) Lai, S. K.; Wu, K. L. *Phys. Rev. E* **2002**, *66*, 041403.
(26) Ito, K.; Yoshida, H. *Colloids Surf. A* **2000**, *174*, 55.
(27) Hachisu, S. *Croat. Chem. Acta* **1998**, *71*, 975.
(28) Russel, W. B. *Nature* **2003**, *421*, 490.
(29) Yethiraj, A.; van Blaaderen, A. *Nature* **2003**, *421*, 513.
(30) Tamai, H.; Fujii, A.; Suzawa, T. *J. Colloid Interface Sci.* **1987**, *116*, 37.
(31) Takayasu, M. M.; Galembeck, F. *J. Colloid Interface Sci.* **1993**, *155*, 16.
(32) Nunes, S. P.; Winkler-Hechenleitner, A. A.; Galembeck, F. *Sep. Sci. Technol.* **1986** *21*, 823.
(33) Kaupp, G.; Herrmann, A. *J. Phys. Org. Chem.* **1997**, *10*, 675.
(34) Kaupp, G.; Herrmann, A. *J. Phys. Org. Chem.* **1999**, *12*, 141.
(35) Kaupp, G.; Herrmann, A.; Haak, M. *J. Phys. Org. Chem.* **1999**, *12*, 797.
(36) Valaskovic, G. A.; Holton, M.; Morrison, G. H. *Appl. Opt.* **1995**, *34*, 1215.
(37) Toledo-Crow, R.; Yang, P. C.; Chen, Y.; Vaez-Iravani, M. *Appl. Phys. Lett.* **1992**, *60*, 2957.
(38) Cardoso, A. H.; Leite, C. A. P.; Galembeck, F. *Colloids Surf. A* **2001**, *181*, 49.
(39) Teixeira-Neto, E.; Galembeck, F. *Colloids Surf. A* **2002**, *207*, 147.